

Wind tunnel pressure data analysis for peak cladding load estimation on a high-rise building

Giulia Pomaranzi^{a,*}, Luca Amerio^b, Paolo Schito^a, Giacomo Lamberti^c, Catherine Gorlé^c, Alberto Zasso^a

^aPolitecnico di Milano, Via G. La Masa 1, 20156, Milan, Italy

^bAdvanced Technology + Research group, ARUP, UK

^cStanford University, Y2E2 Building, 473 Via Ortega, Stanford, CA, 94305

Abstract

A correct evaluation of wind loads on high-rise building cladding panels is essential to ensure safety while avoiding costly over-design. The estimation of peak design loads from wind tunnel tests requires post-processing pressure time histories to remove small-scale fluctuations that do not significantly affect the total load on cladding elements. This post-processing commonly employs a low pass filter with a time-scale that is linearly proportional to the ratio of a reference length scale and velocity. The objective of this study is to analyze the equivalence between the moving-average filter and the spatial averaging procedure, focusing on panels near the top corners and edges of a high-rise building. The real area-averaged pressure is calculated using high-resolution pressure measurements and compared to estimates obtained from moving-average filters with a range of time-scales. The error is within $\pm 1 C_p$ for most pressure tap locations and panels analyzed, although some locations near the top edge result in overestimates of the peak suction up to $3 C_p$. The optimal value of the proportionality coefficient defining the filter time-scale is shown to be dependent on both pressure tap location and panel size, suggesting that accurate estimates of area-averaged pressures based on single-point measurements require more advanced post-processing techniques.

Keywords: Wind Tunnel Tests, Pressure Measurements, Pressure Peak, Cladding Load, TVL

1. Introduction

Recent trends in architecture indicate an increase in the adoption of large glazed panels to cover building façades. In many cases, the governing load for the design of these façades is represented by wind pressure, making the calculation of the wind loads on façade elements a crucial issue. Accurate estimates of these loads are not only relevant from a user safety point of view, but also from an economic point of view: the cladding system can account for up to 25% of the total building cost [1]. In current engineering design, one of the possible ways to estimate the wind design pressure is the application of building codes. Code values are based on wind tunnel test results, and defined to be safely applicable to a wide array of building shapes. As a result, they often provide overly conservative estimates. Wind tunnel tests offer an alternative approach to obtain more accurate results, in particular for high-rise or unusually shaped buildings. These

*Corresponding author

Email addresses: giulia.pomaranzi@polimi.it (Giulia Pomaranzi), luca.amerio@arup.com (Luca Amerio), paolo.schito@polimi.it (Paolo Schito), giacomol@stanford.edu (Giacomo Lamberti), gorle@stanford.edu (Catherine Gorlé), alberto.zasso@polimi.it (Alberto Zasso)

32 tests provide a more detailed understanding of the exact pressure field around the building and avoid costly
33 over-design.

34 The final purpose of a wind tunnel test is the assessment of the design load to be provided to the
35 façade designer. This design load has to represent the maximum correlated pressure over the panel surface
36 area (usually on the order of 5-10 m^2). In principle, its value can be calculated directly from integration
37 of the pressure distribution over the area of interest. However, an accurate measurement of this pressure
38 distribution would require a very dense distribution of pressure sensors that is unattainable in practice. For
39 example, considering a high-rise building facade of 50 m x 100 m covered with panels of 3 m x 3 m,
40 550 panels would be required to cover this single facade. Even just placing one pressure tap at the center
41 of each panel would not be possible in most wind tunnels. Current practice is to distribute the available
42 number of pressure taps over the model surface, paying special attention to the edges and corners. The
43 resulting pressure tap resolution is on the order of one pressure tap every 10 m^2 or more. While this
44 resolution is sufficient when the quantities of interest are the global loads acting on the structure, it results
45 in highly under-resolved measurements of the spatial variability of the pressure field when the cladding
46 loads are to be estimated. At the same time, the high temporal sampling frequency employed in wind
47 tunnel measurements can capture pressure peaks of very short duration. These short-lived pressure peaks
48 are typically characterized by negligible spatial scales compared to the size of a cladding element, indicating
49 they might not be relevant for cladding design [2]. Hence, high-frequency fluctuations that are assumed to
50 not be representative of the total load acting on the panel are usually removed *a posteriori*.

51 A practical approach for estimating the *real* area-averaged pressure acting on an area of interest is to
52 assume that the duration of the peak pressure events is proportional to their spatial extent. This concept of
53 proportionality was first proposed by Lawson [3, 4] to address the fact that at that time most pressure tap
54 measurements were unrelated in time due to limited availability of pressure transducers. Based on full-scale
55 pressure measurements performed by Newberry et al. [5] on Royex House, a high-rise building in London,
56 Lawson suggested relating the averaging time τ to the pressure signal's spatial correlation, specifying τ as
57 proportional to the ratio between the reference length L of the area of interest and the reference velocity V :

$$\tau = \frac{K \cdot L}{V}. \quad (1)$$

58 In this equation, hereafter referred to as the TVL equation, K is a constant representing the exponential
59 decay factor in the spatial coherence function of the pressure signal, with the reduced frequency (computed
60 as fV/L) as independent variable. As such, the τ value computed through Eq.1 represents the load duration,
61 or equivalent time averaging, for which pressure fluctuations are considered to act simultaneously on a
62 surface characterised by a reference length L . The full-scale measurements on the windward face of the
63 Royex House indicated $K = 4.5$. In 1997, Holmes [6] revisited the TVL equation, pointing out that the
64 correlation of the pressure between two points does not provide a measure of the reduction in total load over
65 an area; the total load should be obtained from multiplying the spectral density of a fluctuating point by the
66 local "*aerodynamic admittance*" function [7]. This function can vary from point to point and for different
67 wind directions, depending on the local flow regime. An experimental evaluation of the admittance function
68 would require a spatially-dense distribution of taps, similar to the resolution required to measure the area-
69 averaged pressure distribution itself. Instead, Holmes analytically derived an admittance function based
70 on the assumption of an exponential spatial correlation function. He translated this admittance function
71 into a moving average filter by matching their half-power frequencies, which suggested $\tau = 1.0 \frac{L}{V}$. The
72 resulting moving average filter closely resembled the measured admittance function on Royex house, but
73 this equation is likely to vary considerably for facades other than the windward one [6, 8].

74 The possibility to account for the filtering effect of the area averaging through a very simple expression

75 is the main reason of the popularity of the TVL formula for cladding design, even if its basic assumption of
76 proportionality between the duration and spatial extent of the pressure peaks has not been extensively tested.
77 Recently, Li et al. [9] presented an evaluation of the TVL theory on a 40 m high building roof, focusing
78 on large-scale cladding using an average resolution of 1 pressure tap per 100 m². The results indicate that
79 the value of K varies as a function of the position on the roof, although this conclusion should be further
80 verified for small-scale cladding. Wacker et al. [10] similarly demonstrated that leading edge roof tiles
81 in oblique wind flow revealed significantly reduced spatial correlations that can lead to a reduction of the
82 dynamic wind load. They also considered two cladding panels on a high-rise building and concluded that
83 the pressure signal measured at the centre tap of the panel was representative of the wind load on the total
84 element. However, the panels were located in regions of attached flow, and the temporal resolution of the
85 measurements was much lower than today's standard practice, such that short-lived peak events might not
86 have been resolved. The reduction in spatial correlation observed on the roofs in both studies is attributed to
87 small-scale peak pressure events occurring just downstream of the leading edge of flat (or nearly-flat) roofs.
88 These events have been extensively studied using wind tunnel tests, in particular on low-rise buildings
89 [11, 12, 13, 14, 15]. However, it remains to be investigated whether these peak events, and the related
90 decrease in spatial correlation, could occur in other regions of separated flow, in particular near the corners
91 and edges of high-rise building facades.

92 The objective of the present paper is twofold. First, we aim to provide a detailed analysis of the equiv-
93 alence between the use of a moving-average filter in the time domain and the spatial averaging procedure,
94 including an evaluation of the optimal values of K in the TVL equation. Second, we aim to evaluate the
95 potential of an alternative approach to estimate the area-averaged pressure, using pneumatic averaging over
96 a few pressure taps distributed on a panel. The analysis focuses on locations that are critical for cladding
97 design, i.e. panels near the top corners and lateral edges of a high-rise building façade. Wind tunnel pressure
98 measurements in these locations are available from an experimental campaign performed at the Politecnico
99 di Milano wind tunnel; this data was first presented by Amerio et al. [16] and has been compared and
100 validated against a twin experiment in Florida International University's Wall of Wind (WoW) facility [17].
101 In these experiments, a high-rise building model was instrumented with 448 pressure taps, placed with a
102 very high resolution in two areas of a lateral facade: one located at the top corner, and one located near
103 the edge at half the building height. The resolution of the pressure measurements on these tiles is suf-
104 ficiently high to support an accurate calculation of the *real* area-averaged pressure, allowing comparison
105 to the value obtained using a moving-average filter based on the TVL equation, or to the value obtained
106 from the pneumatic averaging over a few taps. The comparison is performed for different cladding panel
107 sizes, considering a range of values for the filter scaling parameter K for the TVL approach, and different
108 selections of the pressure taps for the pneumatic averaging approach. An additional purpose of the research
109 presented in this paper and in Lamberti et al. [17], is to make the high spatial resolution pressure data set
110 for the determination of cladding loads on high-rise buildings available to the scientific community.

111 The remainder of this paper is organized as follows. Section 2 presents a summary of the experi-
112 mental setup in the Politecnico di Milano wind tunnel, while Section 3 introduces the methodology for
113 post-processing the wind tunnel data. The results are presented in Section 4, first providing an initial com-
114 parison of time histories of the pressure signal, before focusing on peak value analysis based on the TVL
115 and the pneumatic averaging approaches. Section 5 presents the conclusions as well as suggestions for
116 further research.

117 **2. Experimental Setup**

118 The experimental tests were carried out in the Boundary Layer test section of the close-circuit Politec-
 119 nico di Milano wind tunnel. The facility has a cross-section equal to 14 m x 4 m and a length equal to 35 m
 120 (Figure 1). The building model has a rectangular base with dimensions 1 m x 0.3 m and it is 2 m high.
 121 It represents a generic high-rise building at a 1:50 length scale, corresponding to a 100 m tall building at
 122 full-scale. The choice of the 1:50 length scale supports obtaining a realistic representation of the reference
 123 full scale boundary layer profiles (mean velocity, turbulence intensities and integral length scales), while
 124 also enabling an accurate calculation of the area-averaged pressure on a typical cladding panel size given
 125 the pressure tap resolution on the model. The results presented in this paper have also been verified for
 126 a different length scale compatible with the ABL profiles adopted (e.g. using 1:100). The wind speed at
 127 building height was 11.7 m/s in the experiment; considering a full-scale design wind speed of 27.5 m/s, this
 128 implies a velocity scale equal to 1:2.35.

129 The measurements focused on the regions of the building where the highest peak pressures are expected:
 130 two aluminum tiles with 224 pressure taps each were placed in the top corner (tile A) and at the middle of
 131 the vertical edge of the model (tile B). The tap distance is 3 mm close to the building edges and increases
 132 progressively when moving away from the edges. The model was instrumented with 8 PSI ESP-32 HD
 133 high-speed pressure scanners, connected to a data acquisition system with a sampling frequency equal to
 134 500 Hz. The outcome of each test is 300 s (model scale) pressure time histories — corresponding to more
 135 than 3500 convective times referring for normalization to the wind speed at building height and to the 1 m
 136 building width —, measured by the 446 pressure taps. The raw data for the pressure time-histories is post-
 137 processed by dividing the signal by the tubing frequency response function to account for the distortion
 138 introduced by the measurement system. The reference velocity is measured by a Pitot tube located 7 m
 139 upwind to the model. The pitot tube is located 1 m above ground; the measured velocity was corrected to be
 140 representative of the velocity at the building height. Table 1 summarizes the reference length and velocity
 141 as well as the sampling time and frequency at model- and full-scale. The analysis presented in this paper
 142 will focus on incoming wind directions in the range $-15^\circ - +30^\circ$ and $-135^\circ - +150^\circ$, with a 5° resolution,
 143 following the convention shown in Figure 1a.

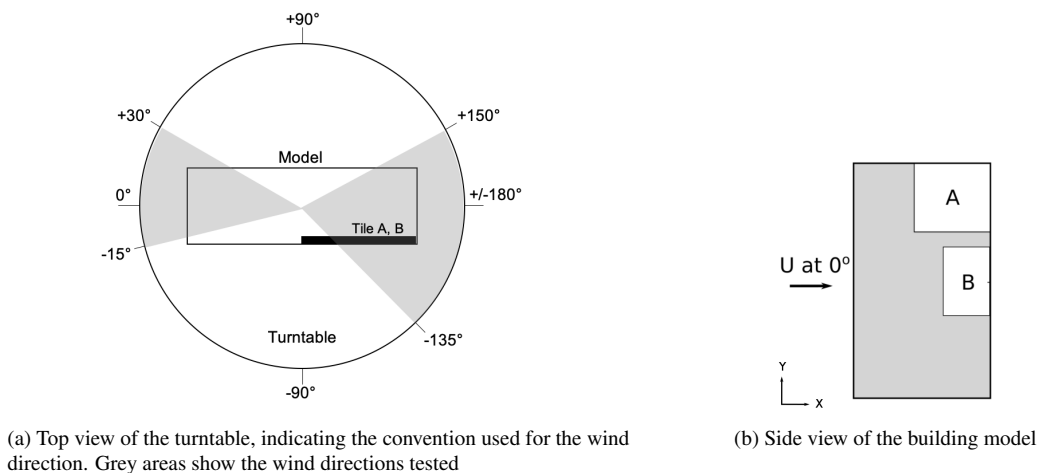


Figure 1: Sketch of the building model.

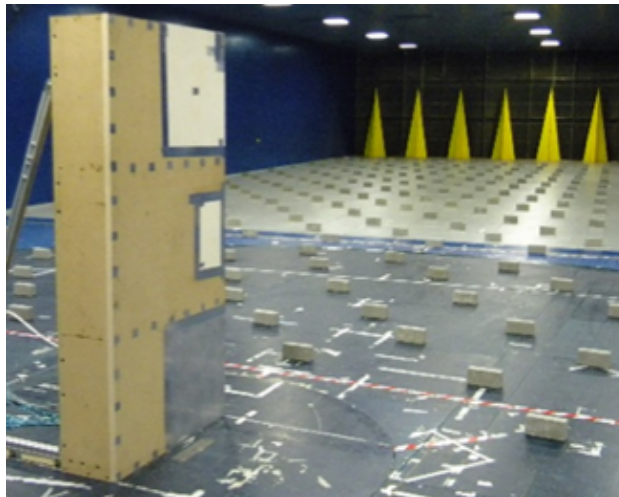


Figure 2: Building model in the Politecnico di Milano wind tunnel test section.

	Model scale	Full scale
H_{ref}	2 m	100 m
$U@H_{ref}$	11.70 m/s	27.5 m/s
Sampling time	300 s	6380 s
Sampling frequency	500 Hz	23.5 Hz

Table 1: Reference height, reference velocity, sampling time and frequency for the wind tunnel tests.

144 *2.1. Flow conditions*

145 Correct scaling of the atmospheric boundary layer is essential to obtain representative wind pressure
 146 measurements on a structure. To generate a representative wind field, the experiments employed passive
 147 turbulence generators (a group of nine 2.5 m tall spires) at the inlet of the test section and roughness elements
 148 (bricks) on the wind tunnel floor upstream of the model, as shown in Figure 2. Velocity measurements were
 149 obtained across the test section at 5 different spanwise locations, spaced 0.6 m and symmetrically arranged
 150 with respect to the centre of the turntable. 20 s time histories of the three velocity components have been
 151 recorded using 3D hot-wires with a sampling frequency of 2000Hz.

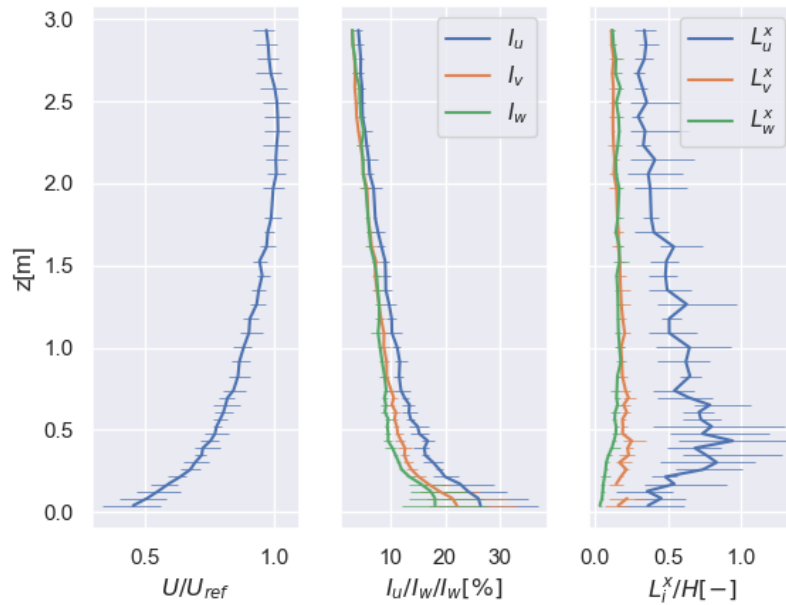


Figure 3: Wind profiles used for the wind tunnel tests. Left: mean speed profile. Centre: Turbulence intensity. Right: Integral length scales. Horizontal bars represents span-wise variation (min-max)

152 Figure 3 shows the resulting mean velocity (left), turbulence intensities (center), and length scales
 153 (right), averaged over the five span-wise locations. The error bars represent the span-wise variability of
 154 each quantity. The mean velocity profile U is normalized with respect to the reference velocity $U_{@H_{ref}}$.
 155 Comparison to a typical logarithmic mean velocity profile indicates that up to 2.4 m height good agreement
 156 is obtained for a roughness length of 1 mm model-scale, corresponding to a z_0/H value of $5 \cdot 10^{-4}$. The
 157 integral length scales are computed using Taylor's hypothesis, taking the product between the mean stream-
 158 wise velocity and the integral time scale obtained from integration of the normalized auto-correlation func-
 159 tion. The resulting length scale profiles differ from the typical ones proposed by the Eurocode or any other
 160 National Code, which normally increase with the height. This discrepancy indicates that the wind tunnel
 161 spectrum will not reflect the larger scales expected in a typical Eurocode spectrum, as is common in larger-
 162 scale model tests [18]. The absence of these larger scales is not expected to have an impact on the results
 163 presented in this paper; it was shown by Tieleman et al. [19] and further discussed by Farell et al. [20]
 164 that the mean and fluctuating pressures on the surfaces of rectangular prisms are primarily controlled by the
 165 small-scale turbulence content of the incident flow and, to a much lesser extent, by the integral scales of the
 166 turbulence, as long as the integral length scale is larger than the length scale of the area of interest (5m at

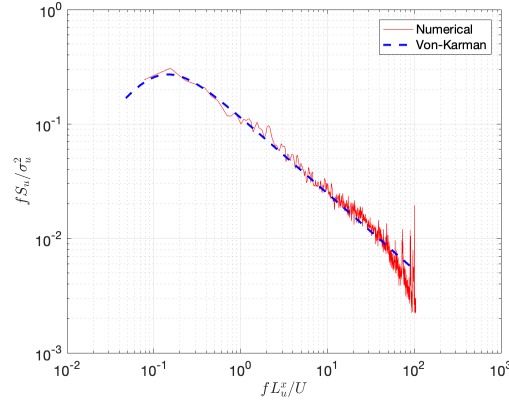
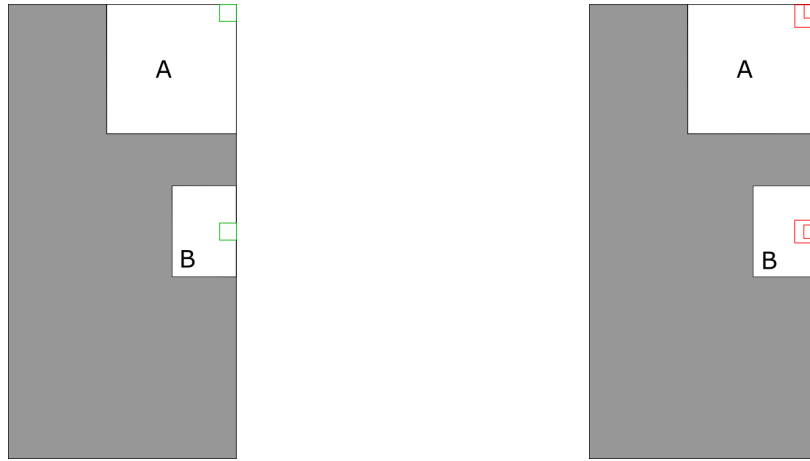


Figure 4: Streamwise velocity spectrum at 1 m height compared to the Von-Karman spectrum



(a) Side view of the building model. The green areas include the 100 taps considered for the analysis.

(b) Side view of the building model. The red squares represent the square panels considered for the analysis, i.e. with 1.5 m, 3 m and 5 m sides at full scale.

Figure 5: Schematic of the analysed regions on the building model.

167 full-scale in this study). The normalized streamwise velocity spectrum measured at 1 m height, shown in
 168 Figure 4, further indicates that a typical ABL turbulence spectrum is obtained; the spectrum compares well
 169 to the Von-Karman spectrum normalized by the measured integral length scale.

170 3. Methodology

171 The objective of this analysis is to assess the accuracy of the TVL approach for estimating the area-
 172 averaged pressure on cladding panels placed on the lateral facade of a high-rise building, at (1) the top
 173 corner, and (2) the edge at half the building height. Specifically, the analysis will focus on the regions
 174 indicated in Figure 5. We will consider the 100 taps closest to the top corner on Tile A, and the 100 taps
 175 closest to the edge at mid-height on Tile B. These regions are known to experience highly negative pressure
 176 peaks [17], and they have a sufficiently high spatial resolution of pressure taps to compute accurate area-
 177 averaged pressures on square panels of three different sizes (sides 1.5m, 3m, and 5m, full scale).

Table 2: Full-scale values of τ [s] for different panel sizes and values of K

	K = 0	K = 1	K = 2	K = 3	K = 4	K = 4.5	K = 5
1.5m x 1.5m	no filter	0.08	0.15	0.23	0.31	0.35	0.39
3m x 3m	no filter	0.15	0.31	0.46	0.62	0.69	0.77
5m x 5m	no filter	0.26	0.51	0.77	1.03	1.16	1.29

178 3.1. Calculation of area-averaged and time-filtered pressure coefficients

179 Throughout this paper, the pressure will be reported in non-dimensional form as a pressure coefficient:

$$C_p(t) = \frac{p(t) - p_{ref}}{\bar{q}_{ref}} \quad (2)$$

180 where p_{ref} is the static reference pressure and \bar{q}_{ref} is the average dynamic pressure measured at building
 181 height, computed as $\bar{q}_{ref} = \frac{1}{2}\rho(\bar{U}_{@H_{ref}})^2$ where ρ is the air density. To support assessing the accuracy of
 182 the time-domain filtering technique and the pneumatic averaging technique, we will consider different time
 183 series derived from the raw pressure coefficient data:

- 184 1. The area-averaged pressure coefficient on a panel, $C_{p,AA}(t)$, calculated as:

$$C_{p,AA}(t) = \frac{\sum_{i=1}^N C_{p,i}(t)A_i}{A} \quad (3)$$

185 where $C_{p,i}$ is the pressure coefficient recorded by the i -th tap, A_i is its influence area and A is the
 186 surface of the panel such that $A = \sum_{i=1}^N A_i$. Since the tributary area of each pressure tap is only few
 187 millimetres wide (model scale), the pressure is assumed to be constant on the tributary area.

- 188 2. The time-filtered pressure coefficient at a pressure tap, $C_{p,\tau}(t)$, calculated by applying a moving
 189 average filter to the raw data. The time span τ of the moving average filter is computed according to
 190 the TVL equation: $\tau = K \cdot L/V$, with L equal to the diagonal of the panel, while V is the reference
 191 velocity at the building height. The value of K is varied from 0, corresponding to the unfiltered raw
 192 data, to 5; the corresponding full-scale values for τ are summarized in Table 2.
- 193 3. The pneumatic-averaged pressure coefficient at a pressure tap, $C_{p,pa}(t)$, calculated by averaging the
 194 signals obtained at 4 or 5 pressure taps on a panel, as depicted in configurations II and III in Figure 6.
 195 Configuration I, which uses the raw data obtained at the center of the panel, is included for reference.

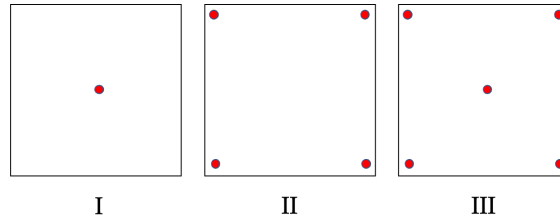


Figure 6: Configurations considered for the pneumatic-averaged pressure

3.2. Calculation of peak pressure coefficients

The presentation of the results will first consider a few snapshots of these different time series before focusing on the resulting estimates of the negative peak values $\check{C}_{p,AA}$, $\check{C}_{p,\tau}$, and $\check{C}_{p,pa}$. The difference between the peak values, $\check{C}_{p,AA} - \check{C}_{p,\tau}$, can then be computed to quantify the accuracy of the design pressure coefficient estimated from a single-point measurement using the TVL approach. Similarly, the accuracy of the pneumatic averaging approach can be determined from the difference $\check{C}_{p,AA} - \check{C}_{p,pa}$. The peak values are calculated following the extreme value analysis proposed by [21]. First, the 10 most negative uncorrelated events are extracted from each time-history, where two events are considered uncorrelated if they are at least 1 second apart in full-scale. Subsequently, these peaks are used to estimate the underlying extreme value parent distribution and compute the expected extreme value over 10 minutes full scale. We note that the resulting values have not been raised to any exponent; following the notation in [21] this corresponds to the use a power-law transformation $Z = X^w$ with $w = 1$. While this approach was originally developed for wind speed data, the underlying statistical methodology is valid for the estimation of the expected peak of any stationary process [22]. The method is also closely related to the Cook and Mayne approach [7].

4. Results

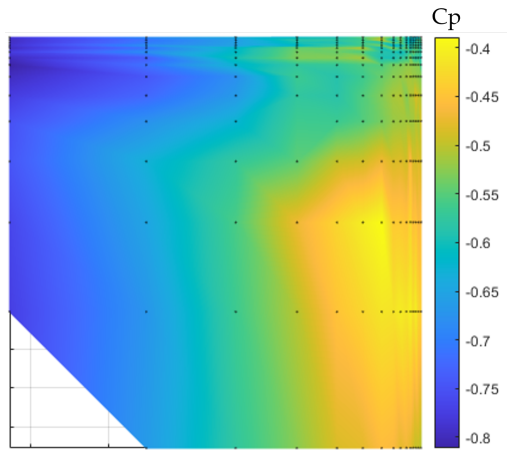
As discussed in Section 3, the presentation of the results focuses on comparing real area-averaged pressure coefficient data to the time-filtered TVL values and the pneumatically averaged values. The first subsection presents snapshots of the time series of C_p to highlight the main qualitative differences between the time series. In the following two subsections, we focus on the quantitative differences in the peak pressure coefficients obtained from the TVL hypothesis and the pneumatic averaging, respectively. Since cladding design is often driven by the negative C_p values (suction), the analysis will primarily focus on the wind directions that cause the extreme suction events, i.e. 10° for Tile A and 180° for Tile B [17]. Figure 7 shows the mean and negative peak pressure distribution on the two tiles for the considered wind directions; the mean negative C_p values indicate that the tiles are in a region of flow separation, with the tile dimension much smaller than the separation region. For Tile A at 10° , the tile is located in the downwind top corner of the facade, while for tile B at 180° , the tile is located just downstream of the upwind corner at the building mid-height. For completeness, the analysis of the TVL hypothesis also includes a presentation of the differences in the envelope peak pressure coefficients that consider the minimum values across all wind directions.

4.1. Comparison of time histories

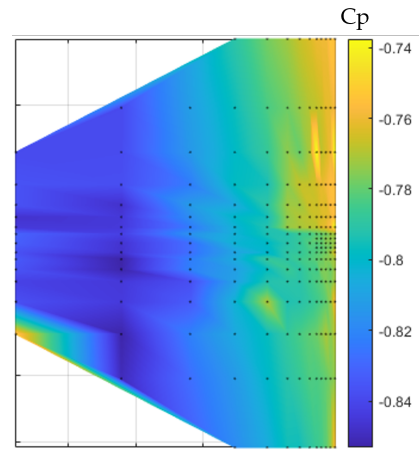
4.1.1. Time histories on Tile A at 10°

Figure 8a presents 4 different snapshots of the time-histories recorded on tile A for the 10° wind direction. It considers a 1.5m by 1.5m panel, and compares the raw data acquired by a pressure tap placed near the top corner of the building to the one obtained using the TVL equation, to the area-averaged value, and to the pneumatically averaged pressure. The TVL approach used a full-scale time span τ equal to 0.34 s, obtained by assuming K equal to 4.5 and L to the diagonal of the panel. The area-averaged value was computed by averaging the signals of the 49 pressure taps available on the panel. Finally, the pneumatic pressure was computed considering Configuration III (see Figure 6), by averaging 5 pressure taps on the panel. Figure 8b shows the same comparison for a 3m by 3m panel size. In this case, the TVL approach used τ equal to 0.69 s, again obtained using K equal to 4.5 and L to the panel diagonal, and the area-averaged value was computed by averaging data from 91 taps. In both figures, the x axis represents model-scale time.

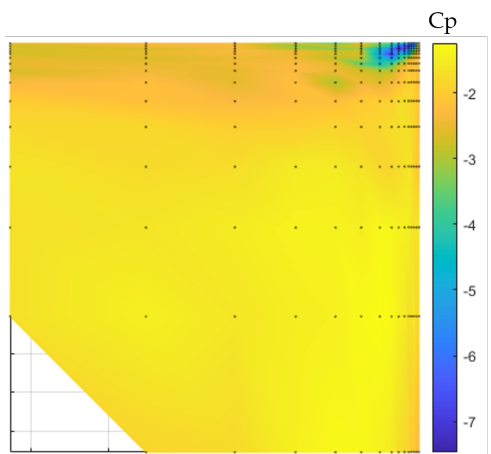
The raw data exhibits several strong negative pressure peaks; the area-averaged time-history shows the same events but with a reduced peak magnitude of approximately 2-3 C_p . This indicates that a large event is



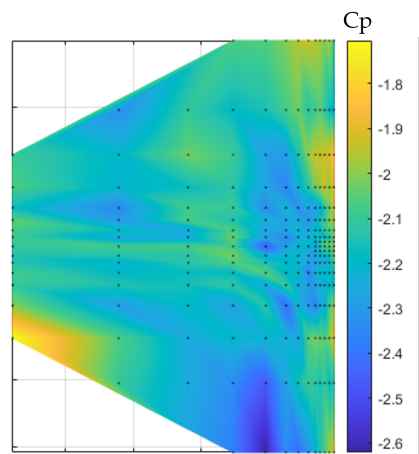
(a) Mean C_p distribution in Tile A, wind direction $+10^\circ$



(b) Mean C_p distribution in Tile B, wind direction 180°



(c) Negative peak C_p distribution in Tile A, wind direction $+10^\circ$



(d) Negative peak C_p distribution in Tile B, wind direction 180°

Figure 7: Mean and peak C_p pressure distribution for Tile A (a, c) and Tile B (b, d)

	Event	raw data	TVL (K=4.5)	area-average	pneum. average
1.5m x 1.5m panel	E1	-4.43	-2.72	-2.36	-2.02
	E2	-4.30	-2.20	-1.48	-1.42
	E3	-4.23	-3.05	-2.02	-1.73
3m x 3m panel	E1	-4.43	-2.00	-1.83	-2.12
	E2	-4.30	-1.53	-1.09	-1.41
	E3	-4.23	-3.06	-1.83	-1.74

Table 3: Comparison of negative pressure coefficients from raw data, from the TVL equation, and from area-average over a panel, and from pneumatic averaging for three suction events (see Figure 8).

239 affecting the entire panel area. During these large events, a shorter event affecting only an extremely small
240 portion of the area with much higher amplitude is observed in the raw data. The latter are too small to affect
241 the area-averaged load as shown by the blue lines in Figures 8a and 8b.

242 Focusing on Figure 8a, a clear difference between the blue line (area-averaged signal) and the pink line
243 (TVL theory) is noticeable during the peak events. The signal processed using the TVL's moving average
244 filter still presents more negative pressure peaks: in some cases, like events E1 and E2 in Figure 8, the peaks
245 have been reduced by the TVL filter compared to the raw signal. However, there are instances, like event
246 E3, where the moving average does not impact the magnitude of the peak. The area-averaged signal does
247 exhibit a reduced peak magnitude, indicating that these events, although longer-lived, are spatially small
248 and do not affect the area-average pressure significantly. Such finding indicates that for these events the
249 ratio between the spatial size and the time duration is much different from the one predicted by the TVL
250 equation: while their duration is larger than the value of τ , their size is much smaller than the panel size.

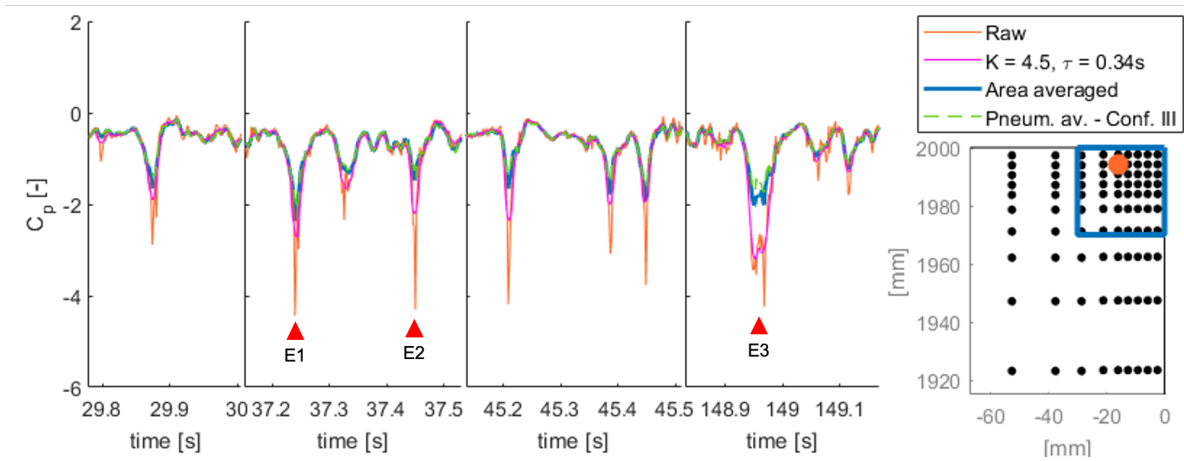
251 The pneumatically averaged signal compares well to the area-averaged pressure in the time intervals of
252 Figure 8. Focusing on peak events E1 and E2, the pneumatic average is able to reflect the area-averaged
253 signal, with a slight overestimation for the 3m side panel. In case of slower event E3, a small discrepancy
254 is found for the 1.5m panel.

255 Table 3 reports the peak values for the two strongest short-lived suction events in the second snapshot
256 (indicated by E1 and E2 in Figure 8), and for the longer duration event in the fourth snapshot (E3 in
257 Figure 8). For the short-lived events on the 1.5m panel, the TVL equation reduces the locally measured
258 peak value by 38% and 49%, while area-averaging results in a reduction of 47% and 66%, respectively.
259 When compared to the pneumatic average values, such reductions increase to 54% and 67%. For the longer
260 duration event, the TVL formula results in a negligible reduction of the peak value over most of the duration
261 of the event, while the area-averaged and the pneumatic averaged values are 50% and 60% lower than the
262 raw data. For the larger 3m panel, the same observation holds: the area-average peak value is significantly
263 lower than the values obtained from the TVL equation.

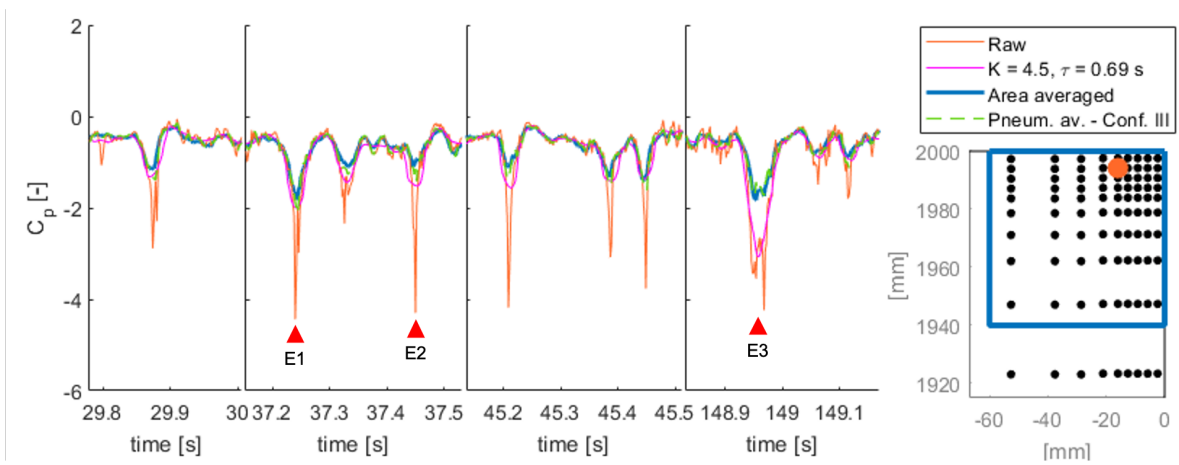
264 Overall, the time series presented in this section indicate that the raw data obtained at a single pressure
265 tap has high-frequency content that is not representative of the pressure acting over the surface area of a
266 cladding panel. The TVL equation with the standard value of K equal to 4.5 fails to make the single tap
267 signal an accurate representation of the area-averaged one; pneumatic averaging over a few taps seems to
268 provide a more representative result.

269 4.1.2. Time histories on Tile B at 180°

270 Considering Tile B for the 180° wind direction, Figure 9 presents a comparison of the raw data acquired
271 by a pressure tap placed at mid-height near the edge of the building to the values obtained using the TVL



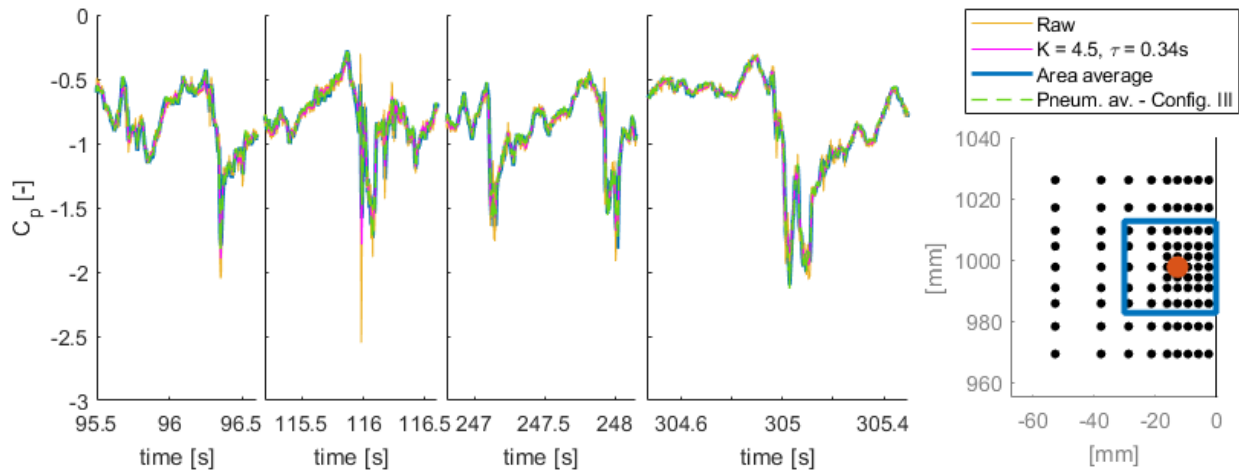
(a) Time histories comparison when the area averaged pressure is computed for a 1.5m by 1.5m panel



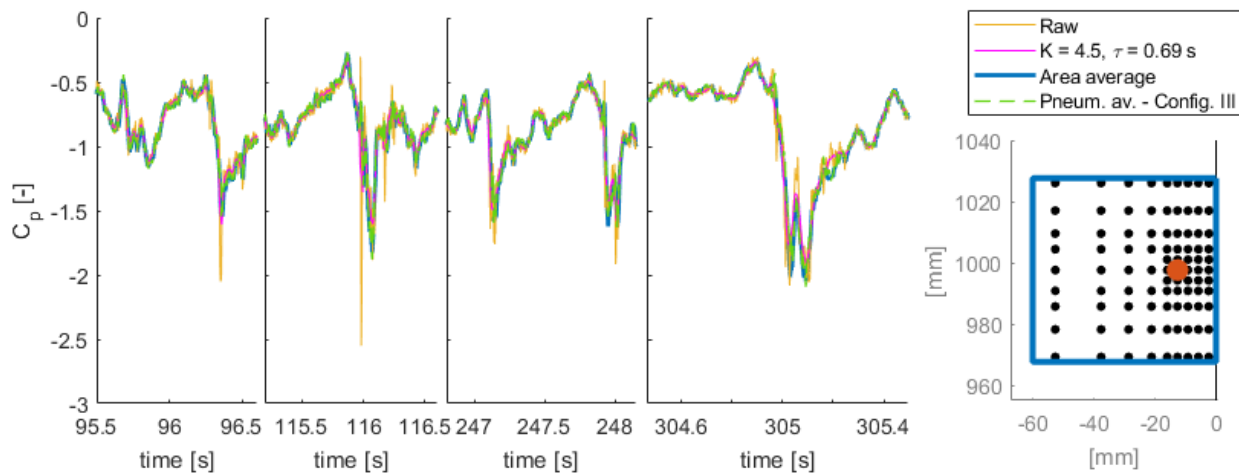
(b) Time histories comparison when the area averaged pressure is computed for a 3m by 3m panel

Figure 8: Comparison between the raw signal of one pressure tap on tile A, the same but filtered by the moving average operator, the area-averaged value, and the pneumatic averaged value on a 1.5m by 1.5m panel (a) and on a 3m by 3m panel (b), wind direction 10° . The maps on the right show the selected pressure tap.

272 equation, to the area-averaged values, and to the pneumatic averaged pressure. The latter is computed
 273 considering 5 taps (Configuration III), as shown in Figure 6. For most of the time, the pressure time series
 274 is largely unaffected by the area-averaging, and the TVL equation produces an accurate representation of
 275 the area-averaged value. Only one event, at $t = 116$ s, is significantly affected by the area-averaging; during
 276 this event the TVL equation remains relatively accurate with $\sim 10\%$ difference in the prediction of the peak
 value. The pneumatic averaged pressure reflects the area-averaged value for any peak event.



(a) Time histories comparison when the area averaged pressure is computed for a 1.5m by 1.5m panel



(b) Time histories comparison when the area averaged pressure is computed for a 3m by 3m panel

Figure 9: Comparison between the raw signal of one pressure tap on tile B, the same but filtered by the moving average operator, the area-averaged value, and the pneumatic averaged value on a 1.5m by 1.5m panel (a) and on a 3m by 3m panel (b), wind direction 180° . The maps on the right show the selected pressure tap.

277 This result is strikingly different from the observations on Tile A for the 10° wind direction. The
 278 raw data is significantly more representative of the pressure acting on a cladding panel, indicating that
 279 the pressure signal in the separation region just downstream of the windward edge has a stronger spatial
 280 correlation. The TVL equation with $K=4.5$ seems to provide an appropriate representation of the area-
 281 averaged value, with the difference between the area-averaged peak events and the ones predicted by the
 282

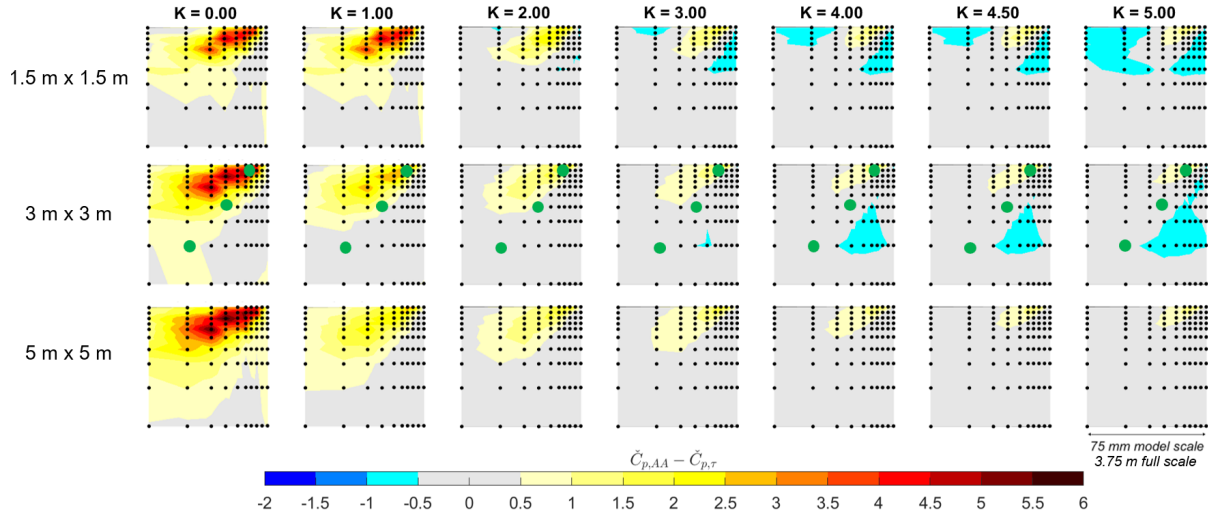


Figure 10: Contour plots of the difference between the values of $\check{C}_{p,AA}$ and $\check{C}_{p,\tau}$ for 10° on Tile A. Green dots show the position of the taps listed in Table 4.

283 filtered signal always less than 10%.

284 4.2. Analysis of time-filtered peak values obtained using the TVL approach

285 In this section, we analyze the difference between the peak values estimated from the area-averaged
 286 signal ($\check{C}_{p,AA}$) and the time-filtered signal ($\check{C}_{p,\tau}$). For the area-averaging, we now consider three panel sizes,
 287 i.e. square panels with a side of 1.5 m, 3 m and 5 m. For the time-filtering, we consider values of K
 288 ranging from 1 to 5. The corresponding values of τ for each panel size are computed according to Eq. 1
 289 and reported in Table 2. This analysis will support identifying if there is a value for K that minimizes the
 290 difference $\check{C}_{p,AA} - \check{C}_{p,\tau}$.

291 4.2.1. Comparison of area-averaged and time-filtered peak values on Tile A - 10° wind direction

292 Figure 10 shows the spatial distribution of the difference $\check{C}_{p,AA} - \check{C}_{p,\tau}$ in the analyzed region of Tile A for
 293 the 10° wind direction. The different rows present the results for the three different panel sizes considered,
 294 while the columns depict different values of K. In this plot, a positive value for $\check{C}_{p,AA} - \check{C}_{p,\tau}$ means that the
 295 peak value computed by applying the TVL theory overestimates the magnitude of the real, area-averaged,
 296 peak value (i.e. $\check{C}_{p,\tau}$ is more negative than $\check{C}_{p,AA}$). Vice versa, a negative difference means that the peak
 297 value computed from the TVL theory is underestimating the magnitude of the area-averaged peak value (i.e.
 298 $\check{C}_{p,\tau}$ is less negative than $\check{C}_{p,AA}$).

299 Figure 10 indicates that using the raw pressure signal ($K = 0$) recorded at taps in the top corner region
 300 leads to severe overestimations of the area-averaged peak pressure magnitudes on a panel: the design value
 301 obtained from the raw data can be more than $5 C_p$ more negative than the area-averaged value for all panel
 302 sizes. The area where these high errors occurs increases with the panel size, since the spatial averaging
 303 operation results in lower peak magnitudes as the averaging area increases. Moving away from the building
 304 corner, the 1.5 m and 3 m cases have some pressure taps that are characterized by small differences, with
 305 $\check{C}_{p,AA} - \check{C}_{p,\tau}$ in the $\pm 0.5 C_p$ range. For the 5 m panel, the differences remains slightly higher over most of the
 306 tile, in the range of $\approx 2 C_p$. Considering the results for $K = 1$, the difference $\check{C}_{p,AA} - \check{C}_{p,\tau}$ decreases, except
 307 for the smallest panel. In this case the time-filtering has a negligible effect since the model scale value of

tap location	$K = 0.0$	$K = 1.0$	$K = 2.0$	$K = 3.0$	$K = 4.0$	$K = 4.5$	$K = 5.0$
close to top corner	4.87	2.82	1.67	1.41	1.24	1.24	1.12
3m panel center	1.01	0.62	0.26	0.077	-0.083	-0.083	-0.17
3m panel edge	0.61	0.31	-0.038	-0.23	-0.38	-0.38	-0.43

Table 4: The difference $\check{C}_{p,AA} - \check{C}_{p,\tau}$ for a tap close to the top corner, for a tap at the 3m panel center and for a tap further away from the building edges (see Figure 10 for tap locations).

308 τ corresponds to only twice the sampling time. As the K value - and, accordingly, τ - further increases,
309 the overestimation of the area-averaged peak pressure further decreases. For the value proposed by Lawson
310 ($K = 4.5$), the TVL estimated extreme values are less than $1 C_p$ different from the area-averaged values in
311 most pressure taps. Only in a small region close to the top corner, where the strongest negative peak events
312 occur, an overestimation of $\sim 1.5 C_p$ is still observed. For the 1.5m and 3m panels, a small (less than $1 C_p$)
313 underestimation of the area averaged peak pressure at a few locations.

314 Table 4 reports the difference $\check{C}_{p,AA} - \check{C}_{p,\tau}$ for three tap locations the 3m panel, indicated by the green
315 dots in Figure 10: a tap close to the building edge, one at the center of the panel and another one placed in
316 the lower left corner of the same panel. The values confirm that taps close to the top corner of the building
317 lead to a severe overestimation of the area-averaged peak pressure for all values of K . Conversely, taps
318 further away from the corner and edges can predict a representative design C_p when the TVL formula is
319 applied, although the optimal value of K is dependent on the tap location.

320 To further visualize how the difference between $\check{C}_{p,AA}$ and $\check{C}_{p,\tau}$ changes with K in different locations, a
321 violin plot [23, 24] is included in Figure 11. The figure only depicts the results obtained for the 3m panel,
322 since the observed trends are representative for all three panel sizes considered in this study. For each value
323 of K , a box plot is shown together with a kernel density plot, estimated for the error population. Each
324 subplot also includes the actual distribution of the error values, where the color of the points indicates the
325 spatial location of the pressure tap following the color code shown in the tile depicted on the right-hand
326 side. The plot identifies three groups of pressure taps, split along the panel diagonal, that behave differently
327 as a function of K . The blue colored pressure taps in the upper triangle exhibit both the strongest spatial
328 dependency and the strongest dependency on the time-filtering. As the value of τ increases, the spatial
329 dependency decreases and the maximum differences $\check{C}_{p,AA} - \check{C}_{p,\tau}$ decrease from more than $5 C_p$ to less than
330 $2 C_p$. For all taps in this group and for all values of K considered, the use of the TVL assumption would
331 result in an overestimate of the peak design load. Moving down to the red taps in the lower triangle along
332 the vertical edge of the building, the results exhibit less spatial dependency as well as a less strong effect
333 of the time-filtering, The differences $\check{C}_{p,AA} - \check{C}_{p,\tau}$ remain in the range $\pm 0.5 C_p$ across all taps in this group
334 for values of $K \geq 1$. The pressure taps in this area define the lower tail of the distribution, resulting in an
335 underestimate of the peak design load for $K > 1$. Lastly, the green pressure taps along the diagonal and
336 farthest from the corner show a behaviour similar to the red taps, but with slightly higher values of $\check{C}_{p,\tau}$. In
337 these locations, the TVL equation provides a good estimate for the peak design pressure using $K \approx 3$.

338 The distinctly different effect of an increase of τ in the upper and lower triangles on the panel suggests
339 a difference in the physical nature of the peak events in these regions. Across the upper triangle, the
340 significant decrease in the variability of the values when τ increases is indicative of short-lived peak events
341 that are strongly reduced by the time-filtering. Across the lower triangle, the reduced influence of τ indicates
342 that the signals are characterized by peak events with a longer duration, for which the time-filtering is less
343 effective. Some pressure taps in the upper triangle consistently exhibit a large value of around $2 C_p$ for
344 $\check{C}_{p,AA} - \check{C}_{p,\tau}$, independently from the value of K considered. It was verified that the dynamic part of the

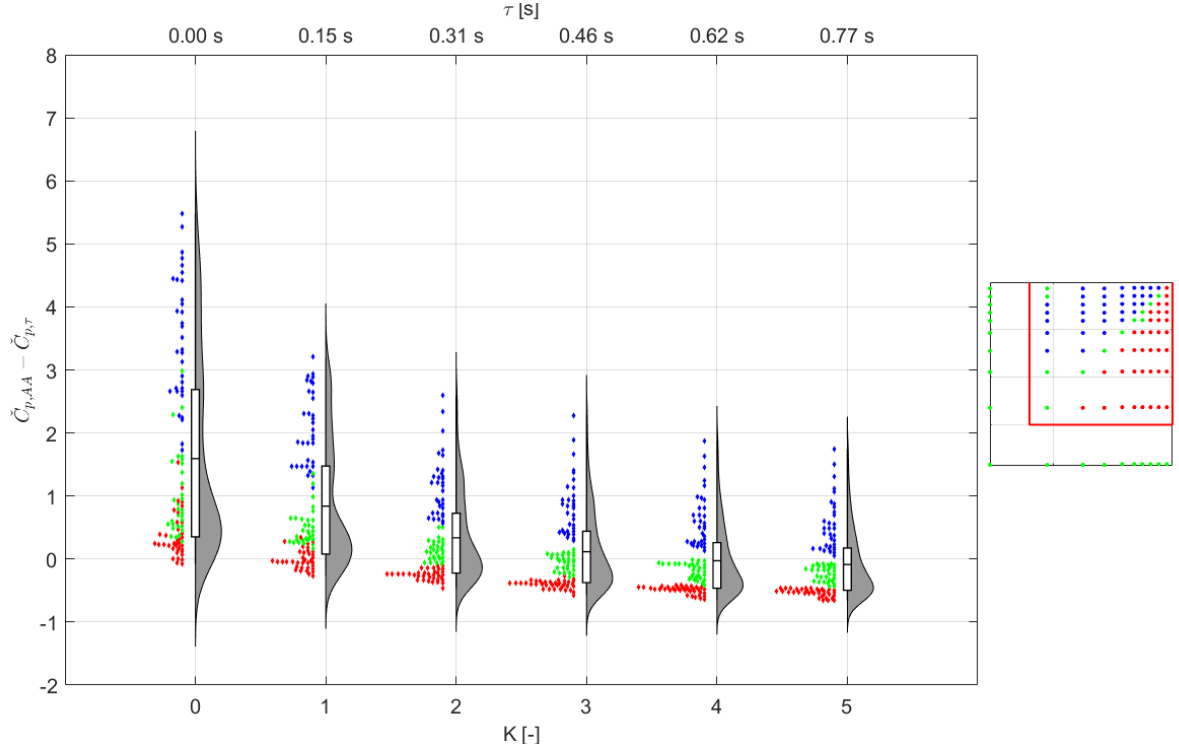


Figure 11: Violin plot of the difference between the values of $\check{C}_{p,AA}$ and $\check{C}_{p,\tau}$ for 10° when a panel size 3m x 3m is considered on Tile A region.

345 signal is the main source of the difference in the peak values by verifying good agreement (within $\pm 0.2 C_p$)
 346 between the mean values of the pressure time series recorded by a single pressure tap and the mean value
 347 of the area-averaged signal. Consequently, the time-averaging procedure using the TVL equation might not
 348 be applicable in the region near the top edge.

349 4.2.2. Tile A - envelope diagrams

350 In the previous sections, the analysis focused on a single wind direction. Since design values are gener-
 351 ally computed as the most negative pressure occurring among all wind directions, this section presents the
 352 envelope diagram. This diagram consider the difference between the lowest value of the area-averaged and
 353 time-averaged peak pressure coefficients among all the wind directions:

$$Err = \min_{\theta} \check{C}_{p,AA}(\theta) - \min_{\theta} \check{C}_{p,\tau}(\theta) \quad (4)$$

354 Using this definition, the minimum area-averaged values across all wind directions are used as the reference
 355 values. It is worth noting that Eq. 4 considers that the most negative values for $\check{C}_{p,AA}$ and $\check{C}_{p,\tau}$ may occur
 356 for different wind directions; this is intentional, since the objective is to analyse the error in the final design
 357 value that is obtained when using time-filtered single pressure tap data versus when using the actual area-
 358 averaged pressure on a panel.

359 Figure 12 shows the contour plots of the difference between the minimum values of $\check{C}_{p,AA}$ and $\check{C}_{p,\tau}$ across
 360 all wind directions. The different rows present the results for the three different panel sizes considered,
 361 while the columns depict different values of K , and correspondingly τ (see Table 2). For $K = 0.0$, i.e. the
 362 raw data, the envelope peak pressure coefficients calculated from the taps experiencing the strongest peak

363 events exhibit the highest difference from the area-averaged values. For the largest panel size considered,
 364 the overestimation reaches a magnitude of $6 C_p$. When increasing the K value, the pressure taps in the
 365 top corner region continue to show positive differences, indicating that the TVL theory still results in an
 366 overestimation of the real area-averaged peak pressure magnitude. This finding holds across all panel sizes.
 367 For pressure taps further away from the corner, an increase in the K value does reduce the difference with
 368 the area-averaged values: in all gray-colored regions, the difference is in the range $-0.5 - 0.5 C_p$. For the
 369 $1.5 m$ and $3 m$ panels, however, several pressure taps exhibit negative values of the difference between the
 370 minimum values of $\check{C}_{p,AA}$ and $\check{C}_{p,\tau}$, in the range -0.5 to $-1.5 C_p$, indicating that in these locations the TVL
 theory results in an underestimation of the envelope design pressure coefficients.

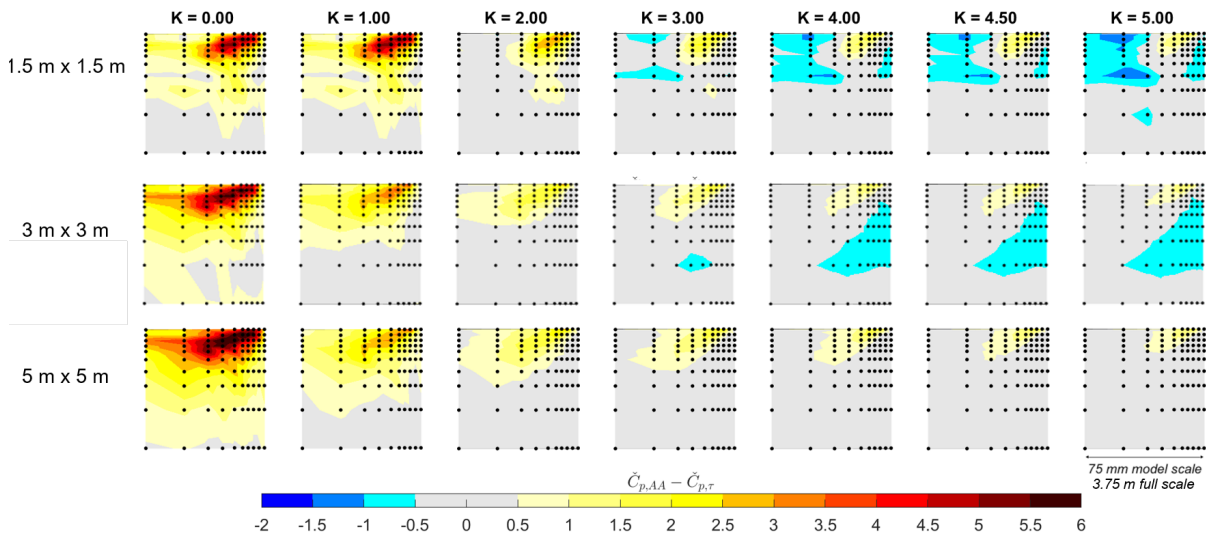


Figure 12: Contour plots of the difference between the minimum values of $\check{C}_{p,AA}$ and $\check{C}_{p,\tau}$ for all wind directions on Tile A.

371 The results in Figure 12 are consistent with those in Figure 10. They indicate that the "optimum"
 372 value of K , i.e. the one that minimizes the difference between the peak value estimated from the time-
 373 filtered signal ($\check{C}_{p,\tau}$) and the peak value estimated from the real area-averaged signal ($\check{C}_{p,AA}$), depends on the
 374 position of the pressure sensor and on the size of the panel. Figure 13 visualizes this dependency through a
 375 contour plot of the value of K that minimizes this difference at each pressure tap. The optimal K value for
 376 the pressure taps near the top edge is up to 5 times higher with respect to other locations. When avoiding
 377 these areas, the optimal K values fall in the range 1 - 4.
 378

379 4.2.3. Comparison of area-averaged and time-filtered peak values on Tile B - Wind direction 180 degrees

380 Figure 14 shows the spatial distribution of the difference $\check{C}_{p,AA} - \check{C}_{p,\tau}$ in the analyzed region of Tile B
 381 for the 180° wind direction. The different rows again present the results for the three different panel sizes
 382 considered, while the columns depict different values of K . Compared to Tile A at 10° , it is worth noting
 383 that the differences between $\check{C}_{p,AA}$ and $\check{C}_{p,\tau}$ assume much smaller values. This could be expected since the
 384 pressure signals on tile B do not exhibit the very strong, but short-lived and localized, peak events observed
 385 on Tile A (see section 4.1 and [17]).

386 For K equal to 0, i.e. when $\check{C}_{p,\tau}$ is equal to the raw signal, the difference with $\check{C}_{p,AA}$ indicates a consistent
 387 overestimate of the area-averaged peak pressure magnitude, but the difference never exceeds $1C_p$. When

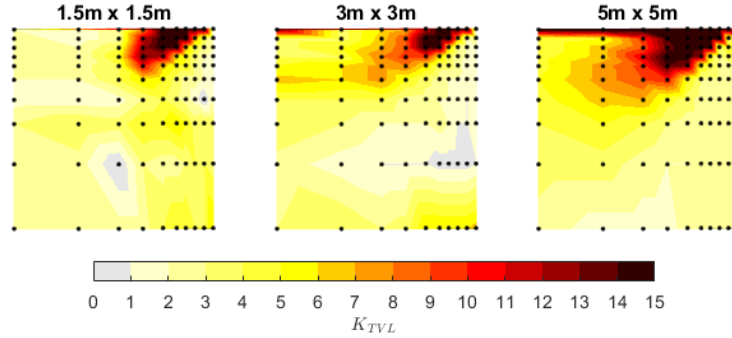


Figure 13: Contour plots of the value for K that minimizes the difference between the minimum values of $\check{C}_{p,AA}$ and $\check{C}_{p,\tau}$ for all wind directions on Tile A.

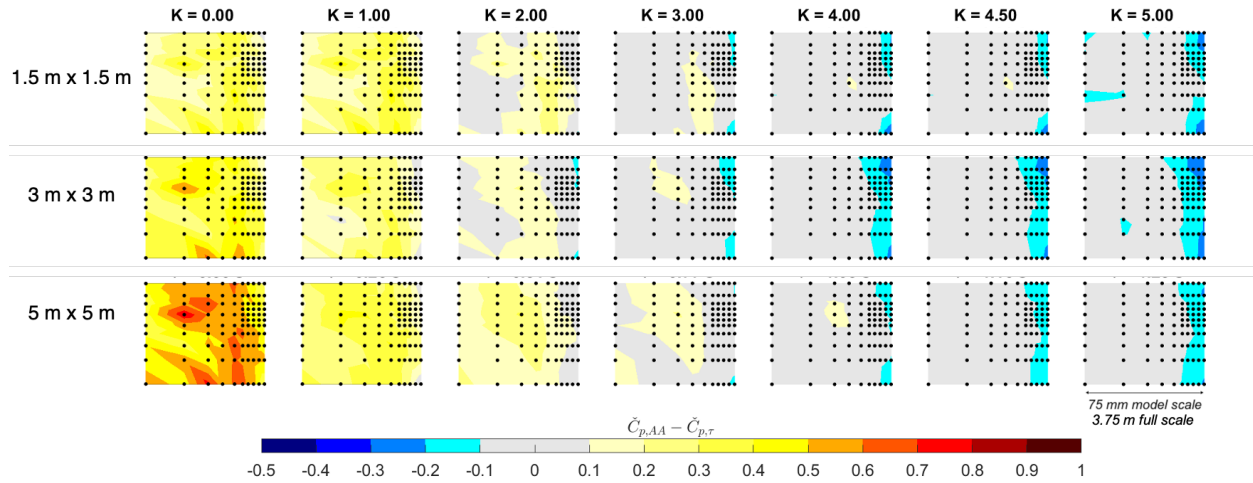


Figure 14: Contour plots of the difference between the values of $\check{C}_{p,AA}$ and $\check{C}_{p,\tau}$ for 180° on Tile B.

388 increasing the K value, the difference starts to assume both positive and negative errors in the range $\pm 0.3C_p$.
 389 For values of K higher than 4, the time series recorded at the taps closest to the building edge lead to an
 390 underestimation of the area-averaged peak values for all the panel sizes considered; the data recorded at all
 391 other taps matches the value of $\check{C}_{p,AA}$ within $\pm 0.1 C_p$.

392 Figure 15 presents the violin plot for the 3m panel to further visualize how the difference between $\check{C}_{p,AA}$
 393 and $\check{C}_{p,\tau}$ changes with K in different locations. For the other panel size, similar behavior was observed.
 394 The plot confirms that for K equal to 0 or 1, $\check{C}_{p,\tau}$ consistently overestimates the area-averaged peak pres-
 395 sure magnitude, but the difference never exceeds $0.7C_p$. When increasing the K value, the value of $\check{C}_{p,\tau}$
 396 decreases, resulting in small differences with $\check{C}_{p,AA}$ in the range $\pm 0.25C_p$. For these higher values of K two
 397 different regions seem to appear: the pressure taps closer to the edge (red dots) form the lower tail, rep-
 398 resenting an underestimation of $\check{C}_{p,AA}$ while those further away from the edge (green dots) form the upper
 399 tail, representing an overestimation of $\check{C}_{p,AA}$. Comparison of the mean values of the pressure time series
 400 recorded by a single pressure tap to the mean value of the area-averaged signal revealed an agreement within

401 $\pm 0.06 C_p$, excluding that differences in the mean values are responsible for such errors. Hence, these two
 402 regions seems to indicate a shift in the dynamic behavior immediately downwind of the windward corner
 vs slightly further downstream, but the differences are far less pronounced than on Tile A.

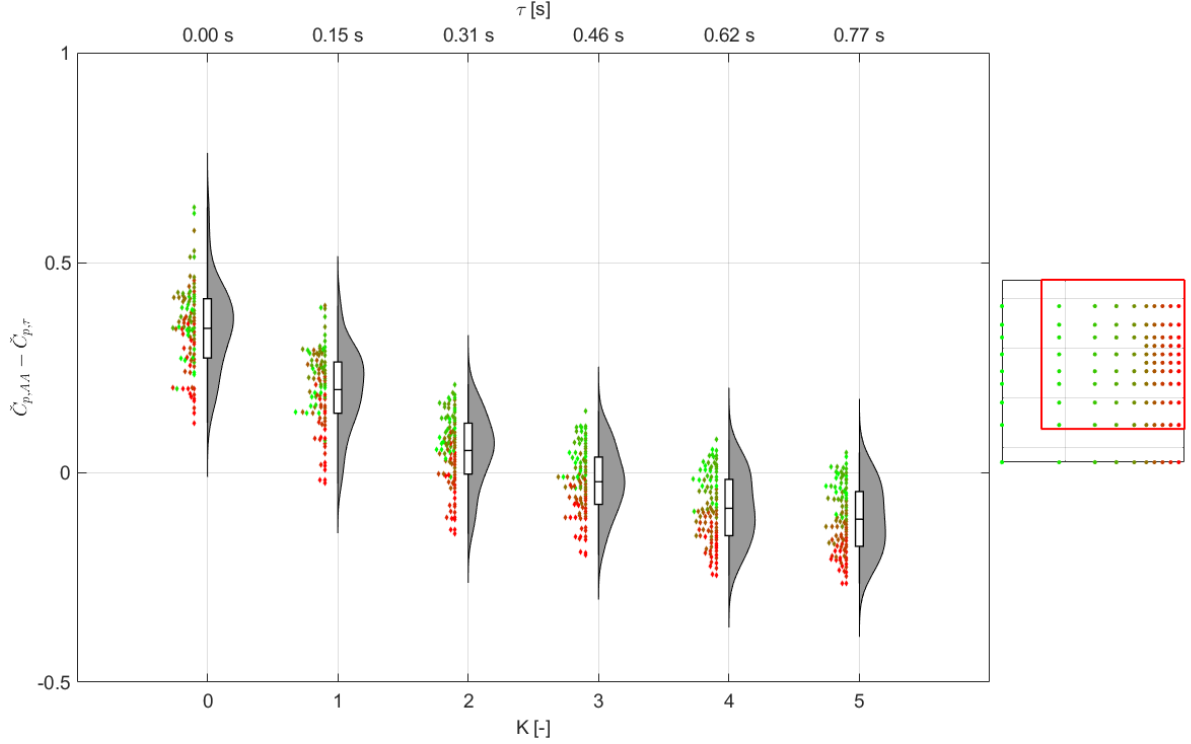


Figure 15: Violin plot of the difference between the values of $\check{C}_{p,AA}$ and $\check{C}_{p,\tau}$ for 180° when a panel size 3m x 3m is considered on Tile B region.

403

4.2.4. Tile B - Envelope Diagram

404 Figure 16 shows the contour plots of the difference between the minimum values of $\check{C}_{p,AA}$ and $\check{C}_{p,\tau}$
 405 across all wind directions on Tile B. The different rows present the results for the three different panel sizes
 406 considered, while the columns depict different values of K , and correspondingly τ (see Table 2). The plots
 407 confirm the findings of the analysis for the 180° wind direction in section 4.2.3: the differences are much
 408 smaller ($< 1.2 C_p$) than on tile A, and they vary from a consistent overestimation of the area-averaged peak
 409 value for $K = 0$ (i.e. using the raw pressure tap data) to a slight underestimation for higher values of K , in
 410 particular for the taps closest to the building edge.

411 Figure 17 presents the contour plot showing the optimal value of K for each pressure tap on the tile B,
 412 for each panel size. In this case, the range of K is limited to 4 - 6, indicating that the original formulation
 413 by Lawson ($K = 4.5$) is adequate for this region at the building mid-height.

4.3. Analysis of pneumatically averaged peak values obtained using a few pressure taps

414 In this section, we analyze the difference between the peak values estimated from the area-averaged
 415 signal ($\check{C}_{p,AA}$) and the pneumatic averaged signal ($\check{C}_{p,pa}$). As in the previous section, we consider three
 416 panel sizes, i.e. square panels with a side of 1.5 m, 3 m and 5 m. For the pneumatic averaging we consider
 417 configurations including 4 and 5 pressure taps, as shown in Figure 6. The case with one single pressure tap
 418 at the center of the panel is also included for reference.
 419
 420

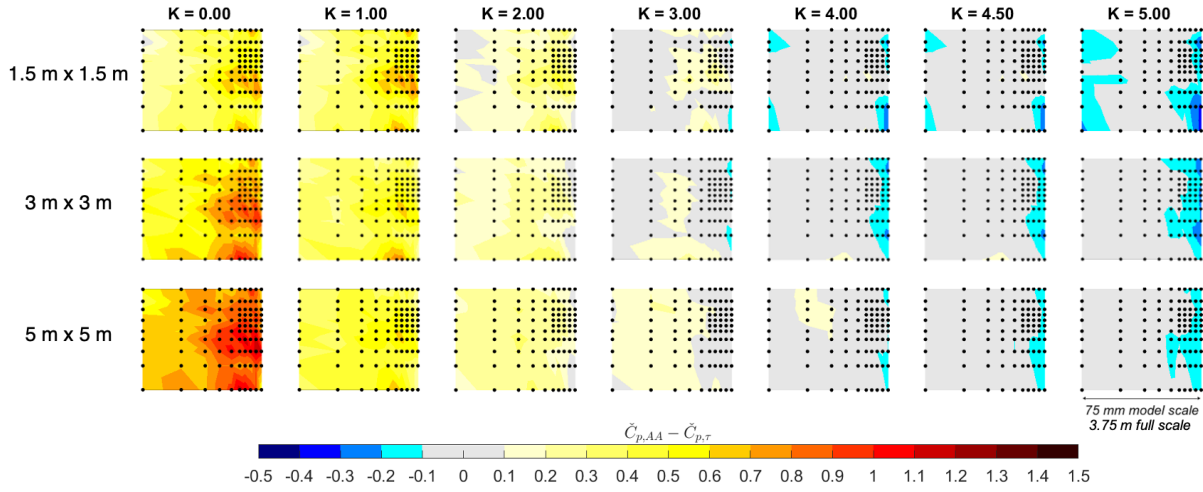


Figure 16: Contour plots of the difference between the minimum values of $\check{C}_{p,AA}$ and $\check{C}_{p,\tau}$ for all wind directions on Tile B.

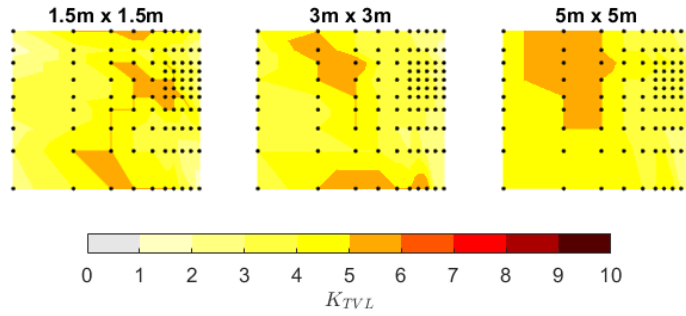


Figure 17: Contour plots of the value for K that minimizes the difference between the minimum values of $\check{C}_{p,AA}$ and $\check{C}_{p,\tau}$ for all wind directions on Tile B.

421 4.3.1. Comparison of area-averaged and pneumatically averaged peak values on Tile A - 10° wind direction

422 Table 5 presents the comparison of the peak pressure coefficients for the top corner of Tile A, consid-
 423 ering the 10° wind direction. Configurations II and III are shown to offer significant improvements in the
 424 estimate of $\check{C}_{p,AA}$ compared to the use of only one pressure tap at the center (Configuration I). The latter
 425 results in an overly conservative estimate of the peak pressure coefficient, with discrepancies between $1C_p$
 426 and $2.5C_p$ for the different panel sizes. In contrast, pneumatic averaging using Configurations II and III
 427 correctly reflects the reduction in the area-averaged peak value as the panel size increases. The difference
 428 between Configurations II and III in terms of peak pressure coefficients is small, indicating that for this
 429 panel location, 4 pressure taps located in the corners of the panel can adequately represent the average
 430 pressure.

Table 5: Comparison of negative peak pressure coefficients of area-average and pneumatic average values for considered configurations on tile A region. Wind direction is 10° .

panel size	$\check{C}_{p,AA}$	$\check{C}_{p,pa I}$	$\check{C}_{p,pa II}$	$\check{C}_{p,pa III}$
1.5m x 1.5m	-2.43	-4.97	-2.16	-2.14
3m x 3m	-1.97	-2.99	-1.72	-1.74
5m x 5m	-1.56	-2.58	-1.43	-1.45

431 *4.3.2. Comparison of area-averaged and pneumatically averaged peak values on Tile B - 180° wind direction*
 432 *tion*

433 Table 6 shows the comparison between the area-averaged peak pressure and the pneumatic averaged
 434 values for panels near the edge of Tile B, considering the 180° wind direction. For this location and wind
 435 direction, the discrepancies when using a single pressure tap at the center range from $0.5C_p$ to $0.25C_p$. When
 436 using the pneumatic averaged pressure obtained with Configurations II and III, the maximum observed
 437 difference is reduced significantly to $0.03C_p$. As on Tile A, the difference between Configuration II and
 438 III is negligible, indicating the 4 pressure taps near the corners can provide a good approximation of the
 439 area-averaged pressure on a tile in this location. The results presented in this section indicate the promising
 440 potential of pneumatic averaging as an alternative to the use of the TVL theory for cladding design wind
 441 tunnel tests.

Table 6: Comparison of negative peak pressure coefficients of area-average and pneumatic average values for considered configurations on tile B region. Wind direction is 180° .

panel size	$\check{C}_{p,AA}$	$\check{C}_{p,pa I}$	$\check{C}_{p,pa II}$	$\check{C}_{p,pa III}$
1.5m x 1.5m	-1.80	-2.05	-1.78	-1.79
3m x 3m	-1.75	-2.07	-1.76	-1.75
5m x 5m	-1.68	-2.18	-1.71	-1.70

442 **5. Conclusions**

443 This paper has presented an analysis of high-resolution pressure tap measurements for peak cladding
 444 load estimation on a high-rise building. The analysis focused on panels near the top corners and edges
 445 of the building's lateral façade, where suction peaks are the determining factor for cladding design. The
 446 high-resolution measurements were used to calculate the real area-averaged pressure on the panels. This
 447 value was then compared to the values obtained using a moving-average filter with a time-scale based on the
 448 commonly adopted TVL equation and to the values obtained using pneumatic averaging over a few pressure
 449 taps on a tile. The comparison was performed for three different cladding panel sizes. The evaluation of the
 450 TVL equation considered a range of values for the filter time-scale $\tau = K \cdot L/V$ by varying K between 0 and
 451 5. Previously proposed versions of the moving average filter have applied $K = 4.5$ (the Lawson formulation)
 452 or $K = 1$ (the Holmes formulation). The evaluation of the pneumatic averaging considered two different tap
 453 configuration, either including 4 taps near the panel corners, or adding an additional tap at the panel center.

454 Considering the panel near the vertical edge at mid-height, the magnitude of the suction peaks is on
 455 the order of $-2 C_p$, and the results support the validity of the TVL equation. In this location, the standard
 456 use of the Lawson formulation results in errors less than $\pm 0.25 C_p$ for all pressure taps considered. The

457 errors primarily result in an underestimate of the peak design load, which is largest when using pressure
458 taps closest to the building edge. In contrast, use of the Holmes formulation results in an overestimate of
459 the peak design load at nearly all pressure taps. The maximum difference of $0.4 C_p$ occurs when using the
460 taps closest to the edge. Use of pneumatic averaging can improve the accuracy of the peak estimates, with
461 errors below $0.03 C_p$.

462 Considering the panel near the top corner, stronger suction events with peaks on the order of $-5 C_p$ are
463 observed, and the results reveal much larger errors when using the TVL equation. The high resolution of the
464 pressure taps allowed to investigate the extremely strong pressure peak events that affect the downstream
465 top corner region on the lateral facade at 10° wind direction. These events were shown to be localized in
466 the area above the corner's bisector line. They are characterized by a spatial size significantly smaller than
467 the panel size, but their duration is longer than what would be expected based on the TVL equation. As a
468 result, the moving average filter does not correctly reduce the magnitude of these peaks in the signal. The
469 standard use of the Lawson formulation would lead to errors in the peak pressure coefficient of $\pm 1 C_p$ in
470 most locations, except for a few pressure taps closest to the top edge and corner where overestimates of up
471 to $2 C_p$ can occur. Use of the formulation by Holmes would mostly result in conservative design values, with
472 overestimates up to $4 C_p$ for pressure taps above the corner's bisector line, and underestimates of less than
473 $0.2 C_p$ for pressure taps below that line. As a potential alternative to use of the TVL equation, pneumatic
474 averaging was found to improve the accuracy of the peak estimates, with errors below $0.3 C_p$.

475 The severe errors that can occur when applying the TVL approach to pressure taps in the top corner
476 region are concerning, because in practice the results between the tap closest to the edge and the adjacent
477 tap that can be several metres (full scale) away are often interpolated. In this case, overestimation of the
478 design pressure by a single tap can cause a large portion of the cladding surface to be overdesigned. In the
479 authors' experience, this type of behaviour and these events have been observed in several commercial wind
480 tunnel tests in proximity of façade vertices, leading to an over-conservative design that negatively impacts
481 the total building costs. A simple workaround could be to avoid to position pressure taps close to the building
482 edges, where the design values obtained using the TVL equation present the largest errors. However, further
483 analysis of the minimum distance at which taps need to be placed under different flow conditions has to be
484 performed. In addition, the results do suggest that the region closest to the building edge is affected by
485 extremely strong suction events with a very limited spatial extension. Hence, any structural/façade element
486 that would be placed in such region should be carefully designed to withstand the corresponding loads.

487 Finally, it is worth considering the implications of the fact that the optimum value of K , i.e. the one
488 that leads to the smallest difference between the estimated peak value and the real area-averaged value,
489 depends both on the location of the pressure tap and on the panel size considered. From a conceptual
490 point of view, this indicates that a moving average time-filter with a time-scale linearly proportional to L/V
491 cannot correctly represent a universal aerodynamic admittance function. At the very least, as also pointed
492 out by Holmes [6], the proportionality coefficient cannot be assumed to be independent of the panel size
493 or the region on the façade considered. In addition to the variability across the building facade, the wind
494 characteristics could further affect the optimal K values reported in this study. The pneumatic averaging
495 approach provided accurate results for all panel sizes and for both locations in this study, which indicates
496 that it could potentially provide a more robust approach to estimating cladding loads near corners and edges.
497 Further research should therefore focus on evaluating the accuracy of the estimates obtained with the TVL
498 hypothesis and with pneumatic averaging considering different high-rise building shapes, different locations
499 on the facades, and different turbulence characteristics.

500 **References**

- 501 [1] M. Overend, K. Zammit, Wind loading on cladding and glazed façades, in: International Symposium on the Application of
 502 Architectural Glass, ISAAG, 2006, pp. 1–10.
- 503 [2] F. Rigo, T. Andrienne, V. Denoël, Mixture model in high-order statistics for peak factor estimation on low-rise building, in:
 504 Conference of the Italian Association for Wind Engineering, Springer, 2018, pp. 613–629.
- 505 [3] T. Lawson, The design of cladding, *Building and Environment* 11 (1976) 37–38.
- 506 [4] T. V. Lawson, *Wind Effects on Buildings: Design Applications*, volume 1, Spon Press, 1980.
- 507 [5] C. W. Newberry, K. J. Eaton, J. Mayne, Wind loading on tall buildings: further results from Royex House, Building Research
 508 Establishment, Building Research Station, 1973.
- 509 [6] J. D. Holmes, Equivalent time averaging in wind engineering, *Journal of Wind Engineering and Industrial Aerodynamics* 72
 510 (1997) 411–419.
- 511 [7] N. J. Cook, The designer’s guide to wind loading of building structures. vol. 2: Static structures, Building Research
 512 Establishment Report, London: Butterworth,— c1990 (1990).
- 513 [8] J. D. Holmes, *Wind loading of structures*, CRC press, 2018.
- 514 [9] D. Li, B. Liu, X. Zhou, Z. Wang, Size effects of area extreme pressure for large-scale cladding, in: *Structures*, volume 29,
 515 Elsevier, 2021, pp. 408–415.
- 516 [10] J. Wacker, R. Friedrich, E. Plate, U. Bergdolt, Fluctuating wind load on cladding elements and roof pavers, *Journal of*
 517 *Wind Engineering and Industrial Aerodynamics* 38 (1991) 405–418. URL: [https://www.sciencedirect.com/science/
 518 article/pii/0167610591900585](https://www.sciencedirect.com/science/article/pii/0167610591900585). doi:[https://doi.org/10.1016/0167-6105\(91\)90058-5](https://doi.org/10.1016/0167-6105(91)90058-5).
- 519 [11] E. Gavanski, Y. Uematsu, Local wind pressures acting on walls of low-rise buildings and comparisons to the japanese and us
 520 wind loading provisions, *Journal of Wind Engineering and Industrial Aerodynamics* 132 (2014) 77–91.
- 521 [12] X. Peng, L. Yang, E. Gavanski, K. Gurley, D. Prevatt, A comparison of methods to estimate peak wind loads on buildings,
 522 *Journal of Wind Engineering and Industrial Aerodynamics* 126 (2014) 11–23.
- 523 [13] D. Banks, R. Meroney, P. Sarkar, Z. Zhao, F. Wu, Flow visualization of conical vortices on flat roofs with simultaneous
 524 surface pressure measurement, *Journal of Wind Engineering and Industrial Aerodynamics* 84 (2000) 65–85.
- 525 [14] J.-X. Lin, D. Surry, H. Tieleman, The distribution of pressure near roof corners of flat roof low buildings, *Journal of wind*
 526 *engineering and industrial aerodynamics* 56 (1995) 235–265.
- 527 [15] J. Lin, D. Surry, The variation of peak loads with tributary area near corners on flat low building roofs, *Journal of Wind*
 528 *Engineering and Industrial Aerodynamics* 77 (1998) 185–196.
- 529 [16] L. Amerio, G. Lamberti, G. Pomaranzi, A. Zasso, C. Gorié, Comparison of high-resolution pressure peaks in closed and
 530 open-section wind tunnels, in: Conference of the Italian Association for Wind Engineering, Springer, 2018, pp. 35–48.
- 531 [17] G. Lamberti, L. Amerio, G. Pomaranzi, A. Zasso, C. Gorié, Comparison of high resolution pressure measurements on a
 532 high-rise building in a closed and open-section wind tunnel, *Journal of Wind Engineering and Industrial Aerodynamics*
 533 204 (2020) 104247. URL: <http://www.sciencedirect.com/science/article/pii/S0167610520301574>. doi:<https://doi.org/10.1016/j.jweia.2020.104247>.
- 534 [18] M. Asghari Mooneghi, P. Irwin, A. Gan Chowdhury, Partial turbulence simulation method for predicting peak wind
 535 loads on small structures and building appurtenances, *Journal of Wind Engineering and Industrial Aerodynamics* 157
 536 (2016) 47–62. URL: <https://www.sciencedirect.com/science/article/pii/S0167610516304202>. doi:<https://doi.org/10.1016/j.jweia.2016.08.003>.
- 537 [19] H. Tieleman, R. Akins, Effects of incident turbulence on pressure distributions on rectangular prisms, *Journal of Wind*
 538 *Engineering and Industrial Aerodynamics* 36 (1990) 579–588.
- 539 [20] C. Farrell, A. K. Iyengar, Experiments on the wind tunnel simulation of atmospheric boundary layers, *Journal of wind*
 540 *engineering and industrial aerodynamics* 79 (1999) 11–35.
- 541 [21] R. I. Harris, Ximis, a penultimate extreme value method suitable for all types of wind climate, *Journal of Wind Engineering*
 542 *and Industrial Aerodynamics* 97 (2009) 271–286.
- 543 [22] E. Gavanski, N. J. Cook, Evaluation of ximis for assessing extreme pressure coefficients, *Frontiers in Built Environment* 5
 544 (2019) 48.
- 545 [23] J. L. Hintze, R. D. Nelson, Violin plots: a box plot-density trace synergism, *The American Statistician* 52 (1998) 181–184.
- 546 [24] Violin plot — Wikipedia, the free encyclopedia, 2021. URL: https://en.wikipedia.org/wiki/Violin_plot.